Hollow silicalite-1 sphere-polymer mixed matrix membranes for gas separation

Beatriz Zornoza[1], Omoyemen Esekhile[2], William J. Koros[2], Carlos Téllez[1], Joaquín Coronas[1,*]

[1]Department of Chemical and Environmental Engineering, Nanoscience Institute of Aragon, Universidad de Zaragoza, 50018 Zaragoza, Spain

[2]School of Chemical and Biomolecular Engineering, Georgia Institute of Technology, Atlanta, Georgia 30332

*Corresponding author: coronas@unizar.es

Abstract

Mixed matrix membranes (MMMs) were prepared combining two different polymers (polysulfone Udel® and polyimide Matrimid®) and hollow silicalite-1 spheres (HZSs) with about 4 μm in diameter. These HZSs were obtained by hydrothermal synthesis from solid mesoporous silica spheres (seeded with silicalite-1 nanocrystals). With filler loadings varying between 0 and 16 wt %, the MMMs were applied to the separation of H_2/CH_4, CO_2/N_2, and O_2/N_2 mixtures. For all the gas ~~pairs~~ mixtures tested, it was found that with a loading of 8 wt % the MMMs performed better than those prepared with pure polymer, other different loadings and conventional silicalite-1 crystals of similar size to that of the HZS diameter. The highest selectivities obtained here for H_2/CH_4, CO_2/N_2, and O_2/N_2 mixtures were 180 (H_2 permeability= 38.4 Barrer), 41.7 (CO_2 permeability= 7.2 Barrer), and 8.5 (O_2 permeability= 2.8 Barrer), respectively.

Keywords: Mixed matrix membrane; Gas permeation; Ordered mesoporous silica spheres; Hollow silicalite-1 spheres; Polysulfone; Polyimide.

1. Introduction

Over the last decade, to establish a membrane with higher gas separation performance relative to the pure polymeric membrane material, various polymers have been changed to produce mixed matrix membranes (MMMs) [1,2] with the incorporation of inorganic fillers, such as zeolites, ordered mesoporous silica, non-porous silica, carbon molecular sieves, and carbon nanotubes. When using nanoporous materials, MMMs have the advantage of combining the benefits of both phases: the superior gas transport properties and thermal resistance of molecular sieves with the desirable mechanical properties, low price and good processability of polymers.

Of the mentioned nanoporous fillers, zeolites are one of the most versatile from the point of view of chemical composition, particle size, shape, and possibility of chemical adaptation for improving interaction with polymer material. A recent zeolitic development includes the layer-by-layer (LbL) procedure used for engineering particle surfaces and fabricating hollow zeolite spheres (HZSs) [3], a new kind of self-bonded molecular sieve structure that have been found application as guest encapsulates [4], controlling release systems [5], and adsorbent materials [6].

Lately, it has been shown that spherical particles of ordered mesoporous silica MCM-41 with narrow particle size distribution (in the 2-4 μm diameter range) would facilitate the preparation of highly homogeneous MMMs [7]. This spherical filler would minimize agglomeration and hence improve dispersability and interaction with the polymer for two reasons: i) the spherical shape limits the contact between silica particles, and ii) the micrometer size spherical particles provide a lower external surface area to volume ratio than that used in other reports (for instance, with approximately 80 nm MCM-41 particles [8]). Alternative approach to obtain MMMs would consist in the use of HZS particles. The obtained HZS-MMMs would benefit from the advantages of

zeolites, as microporous and crystalline molecular sieves, and those of the spherical particles above mentioned. To date, a recent communication has addressed the preparation of HZS-PDMS MMMs [9] and also a few publications use hollow silica spheres for the same purpose of obtaining composite membranes [10,11]. However, there is no detailed report describing the preparation and gas phase application of MMMs using HZSs as filler. Therefore, the aim of this study is the preparation and characterization of HZS-MMMs able to produce an enhancement in terms of selective gas transport. -Even though a considerable research effort has been done on the use of nanoporous materials in polysulfone (PSF)- and polyimide (PI)-based MMMs, a challenge remains when the improvement of permeability-selectivity binomial is taken into consideration for gas mixtures such us H_2/CH_4, CO_2/N_2, and O_2/N_2. Finally, it must be pointed out that HZSs give rise to a new kind of MMM with potential applications no yet studied. As hollow particles they could incorporate a new third encapsulated component to the polymer film. ~~different from the zeolite itself.~~ Then, the membrane could be applied as a drug delivery system, sensor material or active package.

2. Experimental section

2.1 Materials

The chemicals used for the synthesis of mesoporous silica spheres and hollow silicalite-1 spheres were as follows: sodium metasilicate, Na_2SiO_3 (Sigma-Aldrich), cetyltrimethylammonium bromide, CTABr, $C_{19}H_{42}NBr$ (Sigma-Aldrich), ethylacetate, $CH_3COOC_2H_5$ (Sigma-Aldrich), TPAOH, tetra-propyl ammonium hydroxide, 1 M solution (Sigma-Aldrich), and the silica and ethanol source here was TEOS, tetra-ethyl

ortho silicate (98%, Sigma-Aldrich). Polysulfone (PSF) Udel® P-3500 and polyimide (PI) Matrimid® 5218 were kindly supplied by Solvay Advanced Polymers and by Huntsman Advanced Materials, respectively.

2.2 Synthesis of hollow zeolite spheres (HZSs)

Mesoporous silica spheres (MSSs) were synthesized following the experimental procedure given by Schulz-Ekloff et al. [12], but including slight variations in the molar composition of the synthesis sol. [6] To prepare the MSSs used in this work sodium metasilicate, CTABr, and ethylacetate as an initiator for the particles formation were used. The chemicals were mixed in order to obtain a synthesis gel with the following molar composition: 1.5 Na_2SiO_3:1CTABr:361H_2O:7.4$CH_3COOC_2H_5$. Once mixed, the resulting sol was kept in a closed polypropylene flask at room temperature. Whitish color dispersion was achieved 5 h later indicating the silica condensation. Subsequently, the synthesis proceeded at 90 ºC for 50 h in the same open flask, without stirring. The final product was washed several times in distilled water and ethanol, and then filtered. To remove the structural agent from the pores and activate the mesoporous structure MSSs were calcined at 600 ºC for 8 h with heating and cooling rates of 0.5 ºC/min and maintained at 600 ºC.

Silicalite-1 seeds (labeled S1S), approximately 100 nm in size, were prepared by using a sol with the molar composition of 9 TPAOH : 25 SiO_2 : 408 H_2O : 100 EtOH [13] which was autoclaved for 20 h at 100 ºC. To improve the electrostatic interaction between the spheres and the seeds, 2 mL of an aqueous 0.5 M NaCl solution containing 2 mg PDDA (poly (diallyl di-methyl ammonium chloride)) were added to 0.2 g of MSSs dispersed in 2 mL distilled water. Then, to remove the excess of polyelectrolyte, the dispersion obtained was washed with distilled water and centrifuged at 9500 rpm for

20 min four times. The resulting suspension was evaporated at 100 ºC, leaving 2 mL of PDDA-MSS suspension. The PDDA-MSS suspension was placed in contact with 16 mL of diluted NH_4OH (pH= 9.5), and 0.25 wt % silicalite-1 seeds. The excess of silicalite-1 seeds was removed by washing four times with distilled water and centrifugation at 9500 rpm for 20 min. This layer-by-layer seeding procedure was performed only once, producing, in principle, silicalite-1 monolayer coated MSSs. Finally, silicalite-1 seeded MSSs were subjected to hydrothermal synthesis at 448 K for 12 h (the heating time, approximately 0.5 h, is not included) with the following molar composition: KOH : TPABr : 8 SiO_2 : 2130 H_2O [6]. TPABr (tetra-propyl ammonium bromide, 98 %) was purchased from Sigma-Aldrich and KOH (in pellets, 85 %) from Merck. During this synthesis procedure, silica was converted to zeolite giving rise to hollow zeolite (silicalite-1) spheres (HZSs).

To compare, silicalite-1 crystals (labeled S1C) with dimensions of around 0.3 μm x 1 μm x 2.0 μm were also prepared according to a previous work [14]. These crystals were synthesized by hydrothermal growth at 150 ºC for 20 h in a mixture with a molar composition of $5SiO_2$:1TPAOH:$500H_2O$:20EtOH. Subsequently, the mixture was washed by repeating 4 centrifugation steps. All the zeolitic materials (including HZSs) were calcined at 480 ºC for 8 h with heating and cooling rates of 0.5 ºC/min.

2.3 Mixed matrix membrane (MMM) fabrication

Plain PSF and PI membranes were prepared to evaluate their gas separation performance with those of films containing increased amounts of HZSs (loadings of 4, 8 and 16 wt %) as dispersed phase. Before the preparation of the MMMs, the polymers were dried overnight under vacuum (10 mbar) at 100 ºC (for PSF membranes) and 150 ºC (for PI membranes) to remove adsorbed water. To prepare the pure polymer

membranes polymer was dissolved (in a percentage of 10 wt % polymer) in chloroform, allowing good viscosity of the casting solution. This percentage was kept constant for the hybrid membranes. To fabricate MMMs, the synthesized zeolitic materials were dispersed in chloroform (around 90 wt % of solvent-10 wt % combined inorganic filler plus polymer mixture) in an ultrasonic bath for 15 minutes. The polymer (PSF or PI) was then added and the resulted dispersion was magnetically stirred at room temperature for 24 h. Before the membrane casting three intervals of sonication of 15 min were carried out to guarantee a well-dispersed solution. Subsequently, the homogeneous solution was poured on a plain glass surface and left overnight partially covered at room temperature for natural evaporation. The last step was the vacuum treatment under 10 mbar of pressure to remove the solvent remaining within the membrane. The treatment took place in a vacuum oven at 100 ºC for PSF and at 150 ºC for PI, respectively. Membrane thicknesses were measured by a Digimatic Micrometer 0-30 mm (accuracy ±1 μm). For permeation testing membrane circular areas of about 15.2 cm^2 were cut from the films.

2.4 Characterization

MSSs and HZSs were observed by a scanning electron microscope (SEM, JEOL JSM 6400, Jeol Corp. Ltd., Tokyo, Japan, operating at 20 kV) and by transmission electron microscopy (TEM, JEOL-2000 FXII, Jeol Corp. Ltd., Tokyo, Japan, operating at 200 kV). The materials were characterized by X-ray diffraction using a D-Max Rigaku diffractometer with a copper anode and a graphite monochromator to select Cu-$K_{\alpha 1}$ radiation (λ= 1.5418 Å). Low angle X-ray diffraction (LA-XRD) spectra of calcined MSSs were recorded on a Philips X'Pert diffractometer (PANalytical B. V., The Netherlands) with Bragg-Brentano geometry and CuKα radiation.

N_2 adsorption-desorption isotherms of both MSSs and HZSs were measured at -196 ºC using a porosity analyzer (TriStar 3000, Micromeritics Instrument Corp.). The samples were outgassed at 350 ºC for 8 h. BET specific surface areas were measured from the adsorption branches in the relative pressure range of 0.05-0.25 and the pore size distributions were calculated using the Barrett-Joyner-Halenda (BJH) model form the adsorption branches. The sorption properties of the main material examined in this study were tested at 35 ºC for CO_2, N_2, O_2 and CH_4 using a system described elsewhere [15]. Samples (around 30 mg) were pretreated under vacuum overnight at 180 ºC.

SEM MMMs images cross section membranes were observed by previous freeze-fracturing after immersion in liquid N_2, while collecting TEM micrographs needed to embed a portion of the membrane in an Epofix™ cold-setting embedding resin (Electron Microscopy Sciences, Hatfield, PA). For this purpose, 15 parts of embedding resin and 2 parts of hardener (in volume) were mixed and cured during 8 h at room temperature, so that the cross-section pieces could be sliced into the desired sections thin enough to be transparent for the electron beam. The slices were cut at 30-60 nm thickness using a RMC MT-XL ultramicrotome (RMC Products, Tucson, AZ) with a Standard Ultraknife 45º, 3 mm diamond blade (Drukker Ultra-microtome knife, Elementsix™, Cuijk, The Netherlands). The sliced sections were stained in aqueous solution and placed on carbon copper grids for TEM observation.

Thermogravimetric analyses (TGA) were performed using a Mettler Toledo TGA/SDTA 851^e instrument (Columbus, OH). Samples (10 mg) placed in 70 µL alumina pans were heated in air flow up to 850 ºC at 10 ºC/min maintaining the final temperature for 1 h. Differential scanning calorimetry (DSC) measurements were done using a Mettler Toledo DSC822^e equipment (Columbus, OH) to estimate the glass transition temperature (T_g) of the MMMs with growing percentages of MSSs. Small

pieces of dried membranes were transferred to 40 μL aluminum pans, which were hermetically sealed with aluminum covers. The samples were scanned from room temperature to 250 ºC (for HZS-PSF MMMs) and to 400 ºC (for HZS-PI MMMs) with heating rate of 20 ºC/min. Two consecutive runs of this method were performed for each sample and the glass transition temperature (T_g) was calculated from the middle point of the slope transition in the DSC curve. The reported T_g values are the average value based on the second run of 2-3 samples.

Attenuated total internal reflection Fourier transform infrared (ATR-FTIR) spectroscopy of the membranes was performed on a Bruker Vertex 70 FTIR spectrometer (Ettlingen, Germany) equipped with a DTGS detector and a Golden Gate diamond ATR accessory. On the contrary, the sample of powder HZS was prepared by the KBr wafer technique and the measurements were done in a diffuse reflectance module. Both spectra were recorded by averaging 40 scans in the 4000-600 cm^{-1} wavenumber range at a resolution of 4 cm^{-1}. Data were registered with OPUS software from Bruker Optics.

2.5 Permeability measurements

The membranes were tested to separate 50/50 by volume H_2/CH_4, CO_2/N_2, and O_2/N_2 mixtures using a gas permeation setup described elsewhere [7]. The feed mixtures, separately, entered to the membrane through two Alicat Scientific mass-flow controllers (MC-100SCCM-D, Alicat Scientific, Tucson, AZ) (global flow of 50 cm^3(STP)/min)) at pressures above the atmospheric (275 kPa). The membranes were hold into a permeation module which consisted of two stainless steel pieces with a cavity to place additionally a macroporous disk support 316LSS with 20 μm nominal pore size (Mott Corp., Farmington, CT) and gripped Viton® o-rings. The permeate side

of the membrane was swept with a 1 cm^3(STP)/min mass-flow (MC-5SCCM-D, Alicat Scientific, Tucson, AZ) controlled stream of Ar at atmospheric pressure, allowing the transport of gases due to the created different partial pressure. When the CO_2/N_2 and O_2/N_2 mixtures were tested, He was used as the sweep gas. The outgoing concentrations of H_2/CH_4, CO_2/N_2 and O_2/N_2 were analyzed by an on-line gas micro-chromatograph Agilent 3000A (Santa Clara, CA) equipped with TCD. Permeability results were obtained when the exit stream of the membrane was stabilized. The real separation selectivity of both mixtures was calculated as the ratio of experimental permeabilities. Permeabilities are presented in Barrer units (1 Barrer= $1 \cdot 10^{-10}$ cm^3(STP)·cm/(cm^2·s·cmHg)). The permeation measurements were performed at 35 ºC controlled by an UNE 200 oven (Memmert, Schwabach, Germany).

3. Results and discussion

3.1 Morphological and textural characterization

The hollow zeolite spheres (HZSs) used in this work were prepared under the typical synthesis conditions established in a previous work [6]. The HZSs depicted an X-ray pattern similar to that of well-developed silicalite-1 crystals (see Figure S1). These HZSs were prepared from MSSs (Figure 1a) having the ordered mesoporous silica MCM-41 type structure (Figure S2). During the hydrothermal synthesis, the MSSs are completely converted into HZSs. This process is accompanied with an important change in the textural properties of the solids [6]. MSSs have a BET specific surface area of 1023 ±9 m^2/g, whereas HZSs have BET and external specific surface areas of 390 ±13 and 108 ±10 m^2/g. Figure 1b is a SEM image of a HZS particle showing a continuous shell of intergrown silicalite-1 crystals, whereas Figure 1c corresponds to a

TEM image where the black outline would be again the silicalite-1 shell. Figure 1d shows crystal dimensions in the 100 nm range responsible for the external specific surface area quoted above. HZSs not only are quite homogeneous in size but they do not present significant agglomeration even after calcinations at 753 K [6], what is important to achieve well dispersed MMMs. The average measurement by SEM based on more than 30 particles gave us sphere diameters of 3.1 ±0.6 μm for MSS and 4.3 ±0.7 μm for HZS.

To gain insight into the dispersion of the hollow silicalite-1 spheres within the polysulfone (PSF) polymer, MMMs having 0, 4, 8 and 16 wt % of HZSs were prepared. These loadings are below those currently reported in the literature (10-40 wt % [8,16]) where many times no selectivity improvement is observed. Figure 2a shows the SEM appearance of a HZS surrounded by polymer, whereas Figure 2b corresponds to a broken HZS confirming its hollow nature. It is worth noting in both cases the absence of macrovoids as those generated when 2-3 μm zeolite particles are used [17]. Figure 2c shows a TEM cross section observed from 30-60 nm slices obtained with diamond ultramicrotome where the typical coffin growth habit is observed for the silicalite-1 crystals in the shell. The hollow spheres could not afford the shearing generated during the cutting, and the HZS section lost its expected circular shape. On the contrary, the solid mesoporous silica sphere (precursor of HZS) preserved its shape [7].

Even though the HZSs can be of about 4 μm in size, the contact between the polymer and the spheres is made through the small silicalite-1 crystals, around 200 nm in size, constituting the polycrystalline HZSs. In fact, the external specific surface area of these spheres, mentioned above (108 m^2/g), is comparable to that of the silicalite-1 seeds employed for their preparation: 133 ±1 m^2/g with 396 ±2 m^2/g of BET specific surface area. This textural feature is behind the good adherence of the HZSs embedded

in the polymer, not only with PSF (Figures 2a-b) but also when using polyimide (PI) as continuous solid phase (Figure 2d). This adherence is comparable to that of the MSSs (a material whose external surface area is around 1000 m^2/g) dispersed on the same polymer (Figure S3a). Note that silicalite-1 particles with no external specific surface area show (Figure S3b) a poorer interaction with the polymer. The filler distribution is apparently homogeneous and its presence is considerably more evident at the highest loading (see Figures 3a-b). In addition, Figures 3a-c allows one to discard agglomeration between adjacent particles, a phenomenon in which the sphericity of the particles, minimizing the contact between them, play a decisive role. Here the polymer chains enter into the intercrystalline spaces present in the HZS shells, thus giving rise to an interpenetrated zeolite-polymer composite in which a good interaction is expected due to the hydrophobic character of silicalite-1 [18]. This together with the fact that the zeolite particles combined here with PSF and PI polymers are of hollow nature (thus providing empty confined space for the permeating molecules) would give rise to mixed matrix membranes with exceptional permeation features. For comparison Figure 3d shows a MMM made with silicalite-1 crystals.

3.2 Composite characterization

TG analyses in air of HZS-PSF and HZS-PI MMMs with nominal loadings of 0, 4, 8 and 16 wt % were studied. The account of the total accumulated weight loss, in the 83-100 wt % range, allowed the verification of the nominal wt % loading of inorganic filler present in the corresponding MMM, i.e. 4.5, 8.2, and 16.3 wt % residual contents, respectively, for HZS-PSF MMMs, and 4.1, 7.8, and 15.7 wt % for HZS-PI –MMMs. These residual contents are registered as actual loadings (AL) in Table 1.

The glass transition temperature (T_g) corresponds to point that polymer chains change from the rigid to the rubbery state. When MMMs were prepared with HZSs, there was a continuous increase in T_g as the MSS mass fraction increased, namely 8.2 and 25.5 ºC differences for PSF and PI polymers: from 188.5 ºC at 0 wt % to 196.7 ºC at 16 wt %, and from 316.7 ºC at 0 wt % to 342.2 ºC at 16 wt% (see Table 1), respectively. Analogous T_g variations from 188.5 to 199.5 ºC for 0-32 wt % mesoporous silica spheres-PSF MMMs [7], and from 317 to 340 ºC for 0-30 wt % mesoporous ZSM-5-PI MMMs [16] have recently been reported. This is consistent with increasing rigidity and restricted motion of the polymer due to the chemical interactions established between chain polymer and HZS external surface area, and agrees with the fact that the filler-polymer interaction here is comparable to that of composites with higher mesoporosity. Note that T_g values for Udel® P-3500 and Matrimid® 5218 reported in literature [19] are 182 ºC and 313 ºC, respectively.

The FTIR spectra obtained from the different materials (Figure S4) suggest interactions via hydrogen-bonding between the OH groups in the zeolite (which would be related to the external specific surface area above evidenced for the HZSs) and the aryl (Ar) ether and carbonyl groups in PSF and PI, respectively. These interactions with the two polymers translate into weak shifts linked to the Ar-O-Ar (1235 cm^{-1}) and S=O (1294 cm^{-1})) groups in the case of PSF [20] and the C=O (1673-1779 cm^{-1}) in the case of PI [21].

3.3 Gas separation performance

The performance of the MMMs containing HZSs was tested in the gas phase separation of H_2/CH_4, CO_2/N_2 and O_2/N_2 mixtures. The O_2/N_2 membrane separation corresponds to the most investigated gas pair, while the other two can be related to H_2

purification and CO_2 capture, probably two of the most important gas phase separation processes of nowadays. The MFI-type structure of silicalite-1 has straight channels with a pore opening of 0.54 x 0.56 nm along its b-axis and sinusoidal channels of 0.51 x 0.55 nm along its a-axis [22]. This, together with its hydrophobicity (allowing a good interaction with polymers), is the reason why this zeolite has been used as filler for MMMs, sometimes combined with polysulfone [23] and polyimide [24].

The addition of microporous fillers often decreases the gas permeability of MMM [25]. However, the HZS phase used here with empty internal space may favor gas diffusivity, and causes the H_2 permeability to increase with the HZS loading (see Figure 4). In fact, the empty spaces provided by the HZS are somehow similar to those generated by the disruption of polymer chain packing and linking due to the presence of certain fillers [26] which lead to an increase in polymer free volume. Moreover, due to a molecular sieving effect H_2 diffuses faster than CH_4 because of its smaller kinetic diameter (0.29 vs. 0.38 nm), and the H_2/CH_4 selectivity increases up to a loading of 8 wt %. Loadings lower than 8 wt % HZS did not alter significantly the MMM transport properties benefiting from the increase in rigidity of the polymer matrix (in agreement with the previous observation of T_g variation) and the diffusion selectivity expected through the silicalite-1 microporosity, which favor H_2 over CH_4 diffusion. In fact, diffusivities for H_2 and CH_4 are in silicalite-1 (estimated at 35 ºC) $6.6 \cdot 10^{-9}$ and $1.3 \cdot 10^{-9}$ m^2/s, respectively [27]. At higher HZS loadings, by-passing channels might connect surrounded voids existing between silicalite-1 spheres particles, as the 16 wt % HZS MMMs selectivity values close to those of the pure polymers suggest.

In addition, the positive effect of the filler formulated here is demonstrated for both PSF and PI polymers with the advantage of the later to be~~of being~~ more permeable membrane material. As shown in Figure 4, the highest H_2/CH_4 selectivity was 180 (that

corresponds to a value of H_2 permeability of 38.4 Barrer) for 8 wt % HZS-PI MMM, while the highest H_2 permeability was 49.3 Barrer (together with a H_2/CH_4 selectivity of 130) for 16 wt % HZS-PI MMM. It is worth mentioning that both H_2 permeability and H_2/CH_4 selectivity were 30.4 Barrer and 132 for pure PI, respectively. To illustrate our fair approach to membrane characterization, these values are compared to ~~in Table 2 with~~ those corresponding to pure PI [28,29] and PSF [30,31], and with those achieved with ZSM-5-PI MMMs [16] in Table 2. ZSM-5 has the same MFI-type structure than silicalite-1 membranes. Finally, the increase in permeability with the load suggests that the penetration of the polymer chains would not affect the interior of the silicalite-1 spheres.

Good results were also obtained for the separation of the CO_2/N_2 (Figure 5) and O_2/N_2 (Figure 6) mixtures with the composite membranes. Given their interest, these are two mixtures that have been previously studied with pure PSF [32] and PI [16] membranes, PSF- and PI-based MMMs [16,32,33], and even with pure silicalite-1 [34,35] membranes. The relatively small difference in kinetic size ~~there exist~~ between CO_2 (0.33 nm) and N_2 (0.36 nm) is consistent with close polymer diffusivities for both molecules for pure PSF [30-32] and pure PI [16,33]. The CO_2 selectivity must be attributed to differences either of solubility or of adsorption. In fact, the solubility coefficients are higher for CO_2 than for N_2 in both PSF [30-32,36] and PI [16,33] polymers. Thus, in the case of PSF [30-32,36], even CO_2/N_2 diffusivity selectivity is slightly lower than one; CO_2/N_2 solubility selectivity is 26.8, giving a permeability selectivity of 26.6. This value is close to the CO_2/N_2 selectivity measured in this work as permeabilities ratio for bare PSF membranes (24.3).

Concerning the filler, silicalite-1 has saturation capacities for CO_2 and N_2 of 5.0 and 5.4 mmol/g, in good agreement with the values calculated here for HZSs (shown

later), while CO_2 and N_2 diffusivities were for silicalite-1 [27] estimated at 35 ºC $1.6 \cdot 10^{-10}$ vs. $1.5 \cdot 10^{-9}$ m^2/s, respectively. More relevant in this case is the adsorption enthalpy, which clearly favors CO_2 (24.1-27.4 kJ/mol) over N_2 (13.8-18.5 kJ/mol) [27,37,38] and justifies the use of the zeolite as filler for this separation. In fact, based on CO_2-preferential adsorption, MFI-type zeolite membranes have been successfully applied to separate CO_2/N_2 mixtures [35,39]. Again, the best selectivity value can be found at 8 wt % loading. As shown in Figure 5, the highest CO_2/N_2 selectivity was 41.7 (CO_2 permeability= 7.2 Barrer) for 8 wt % HZS-PSF MMM, while the highest CO_2 permeability was 21.7 Barrer (CO_2/N_2 selectivity= 25.5) for 16 wt % HZS-PI MMM. Table 2 compares these values with those achieved with~~corresponding to~~ pure PSF [8,30,31], pure ~~and~~ PI [16,28,29], and ~~with those achieved with~~ ZSM-5-PI MMMs [16].

Since both O_2 and N_2 are (from the point of view of diffusion and adsorption) more similar molecules than the other two tested pairs, the achievements with the O_2/N_2 mixture were more modest but also noticeable. As in many other previous reports related to pure polymer and mixed matrix membranes, the starting points (permeability-selectivity) are lower than for the other two mixtures, and O_2 permeability is higher than that of N_2 [16,32,33]. Figure 6 shows again ~~the~~ a ~~best~~ maximum O_2/N_2 selectivity of 8.5 (O_2 permeability= 2.8 Barrer) ~~at~~ with 8 wt % loading (8 wt % HZS-PI MMM), while the highest O_2 permeability being 4.5 Barrer (O_2/N_2 selectivity= 6.0) for 16 wt % HZS-PI MMM. These values were also compared~~s~~ with those corresponding to pure PSF [8,30,31] and PI [16,28,29], and the ones ~~with those achieved~~ with ZSM-5-PI MMMs [16]. Finally, Tables S2-S4 show the values for the permeabilities and selectivities obtained in this work. The figures in these tables are the average of 2-4 separation experiments with different samples.

To justify the special filler used here to prepare MMMs, conventional silicalite-1 crystals (S1C) were used at the 8 wt % loading with both PSF and PI polymers. The results can be seen as open symbols in Figures 4 to 6 for the H_2/CH_4, CO_2/N_2 and O_2/N_2 mixtures, respectively. As expected, in most of the cases S1C-polymer membranes performed better than the corresponding pure polymer. However, when the comparison is done between HZS- and S1C-polymer membranes at the same loading level of 8 wt %, the HZS-MMMs always present higher selectivity and permeability. The improvement in selectivity is attributed to the good bonding established between the polymers and the external roughness of hollow silicalite-1 spheres that are composed of tens of intergrown crystals. The improvement in the permeability might be related not only to the free volume generated ~~for~~ by the disruption of the polymer chains (something also produced by S1C) but also to the hollow space present in each HZS particle. Figure 7 represents this idea: molecules that selectively permeate in the hollow filler can pass through it more easily than molecules whose diffusion or adsorption is not favored by the zeolite. Finally, it is worth mentioning that MSS-MMMs [7] prepared combining mesoporous silica spheres and PSF (open triangles in Figures 4 and 5 for H_2/CH_4 and CO_2/N_2 mixtures) showed better performance at least in terms of permeability and for the same load of filler (8 wt %).

In order to better understand the results shown above, the O_2, N_2, CH_4 and CO_2 adsorption isotherms were measured at 35 ºC for HZS powders. The obtained results were fitted to the Langmuir equation (Figure 8):

$$\theta = \frac{K_A P_A}{1 + K_A P_A} \xrightarrow{\text{linearization}} \frac{1}{q} = \frac{1}{q_M} + \frac{1}{q_M \cdot K_A}\frac{1}{P_A} \qquad (1)$$

where $\theta = q/q_M$ is the fractional coverage of the surface of the solid adsorbent; q, the adsorbed amount (mmol/g) at the adsorbate partial pressure P_A (kPa); q_M, the maximum amount (mmol/g) that can be adsorbed on the surface of the solid; and K_A (kPa^{-1}), the

adsorption equilibrium constant of certain adsorbate A on the surface [40]. Parameters q_M and K_A can be obtained from the linearization of this equation and the plot of the inverse of q vs. the inverse of P_A. Saturation capacities (q_M) are for N_2, CH_4, and CO_2 4.5, 4.8, and 4.1 mmol/g, respectively. These values are in consensus with those reported by Bakker *et al.* [27] and discussed above. Additionally, because the polymer chains (about 1 nm in size [7]) cannot enter into the silicalite-1 microporosity, these adsorption results suggest gas transport through the filler studied here.

The improvement achieved by the HZS-polymer MMMs in the CO_2/N_2 separation is in good agreement with the higher CO_2 adsorption capacity that the HZS particles show in Figure 9. In fact, CO_2 q_M values are for mesoporous silica spheres (MSS), silicalite-1 crystals (S1C), and hollow zeolite spheres (HZS) 3.9, 4.4, and 4.8 mmol/g, respectively.

4. Conclusions

Mixed matrix membranes of well-dispersed hollow silicalite-1 spheres and two different polymers (polysulfone Udel® and polyimide Matrimid®) can be prepared and efficiently used in the separation of H_2/CH_4, CO_2/N_2, and O_2/N_2 gas mixtures. Even though some features continuously increased (the glass transition temperature) or monotonically evolved (SEM and TEM appearance and TGA analyses) with filler loading, the best permeability-selectivity binomial was obtained at 8 wt %.

From the point of view of the selectivity towards a given separation, the good behavior of the hollow silicalite-1 spheres-mixed matrix membranes studied here is attributed not only to the microporosity of the filler but also to the good bonding between the polymers and the external surface of hollow silicalite-1 spheres (composed of tens of intergrown crystals). However, at certain filler loading the selectivity

decreases. On the other hand, the improvement in the permeability relates not only to the free volume generated for the disruption of the polymer chains (something also produced by the conventional silicalite-1 crystals), the hollow space present in each HZS particle contributes too. Table 3 summarizes the advantages of the membranes prepared here, discussed along the paper but also elsewhere [7] when MSS-MMM were studied alone.

Acknowledgement

Financing from the Spanish Ministry of Science and Innovation (MAT2007-61028, CIT-420000-2009-32) is gratefully acknowledged. B. Zornoza also acknowledges the funding from the Spanish Ministry of Education and Science (FPU Programme) and Fundación Ibercaja. Dr. N. Navascués is thanked for help with HZSs preparation.

References

[1] T.S. Chung, L.Y. Jiang, Y. Li, S. Kulprathipanja, Mixed matrix membranes (MMMs) comprising organic polymers with dispersed inorganic fillers for gas separation, Prog. Polym. Sci. 32 (2007) 483-507.
[2] P. Bernardo, E. Drioli, G. Golemme, Membrane Gas Separation: A Review/State of the Art, Ind. Eng. Chem. Res. 48 (2009) 4638-4663.
[3] L. Tosheva, V.P. Valtchev, Nanozeolites: Synthesis, Crystallization Mechanism, and Applications, Chem. Mater. 17 (2005) 2494-2513.
[4] A.G. Dong, Y.J. Wang, Y. Tang, N. Ren, Y.H. Zhang, Z. Gao, Hollow zeolite capsules: A novel approach for fabrication and guest encapsulation, Chem. Mater. 14 (2002) 3217-+.
[5] D.J. Wang, G.B. Zhu, Y.H. Zhang, W.L. Yang, B.Y. Wu, Y. Tang, Z.K. Xie, Controlled release and conversion of guest species in zeolite microcapsules, New J. Chem. 29 (2005) 272-274.
[6] N. Navascues, C. Tellez, J. Coronas, Synthesis and adsorption properties of hollow silicalite-1 spheres, Microporous Mesoporous Mat. 112 (2008) 561-572.
[7] B. Zornoza, S. Irusta, C. Tellez, J. Coronas, Mesoporous Silica Sphere-Polysulfone Mixed Matrix Membranes for Gas Separation, Langmuir 25 (2009) 5903-5909.
[8] S. Kim, E. Marand, High permeability nano-composite membranes based on mesoporous MCM-41 nanoparticles in a polysulfone matrix, Microporous Mesoporous Mater. 114 (2008) 129-136.

[9] K. Vanherck, A. Aerts, J. Martens, I. Vankelecom, Hollow filler based mixed matrix membranes, Chem. Commun. 46 2492-2494.
[10] J.J. Yuan, G.B. Zhou, H.T. Pu, Preparation and properties of Nafion (R)/hollow silica spheres composite membranes, J. Membr. Sci. 325 (2008) 742-748.
[11] L.P. Wang, L.M. Zhao, W.Z. Li, Fabrication of polymer-hollow sphere optical-functional hybrid material via RAFT polymerization, React. Funct. Polym. 70 (2009) 35-40.
[12] G. Schulz-Ekloff, J. Rathousky, A. Zukal, Mesoporous silica with controlled porous structure and regular morphology, Int. J. Inorg. Mater. 1 (1999) 97-102.
[13] S. Mintova, T. Bein, Microporous films prepared by spin-coating stable colloidal suspensions of zeolites, Adv. Mater. 13 (2001) 1880-1883.
[14] Z.P. Lai, G. Bonilla, I. Diaz, J.G. Nery, K. Sujaoti, M.A. Amat, E. Kokkoli, O. Terasaki, R.W. Thompson, M. Tsapatsis, D.G. Vlachos, Microstructural optimization of a zeolite membrane for organic vapor separation, Science 300 (2003) 456-460.
[15] T.T. Moore, W.J. Koros, Gas sorption in polymers, molecular sieves, and mixed matrix membranes, J. Appl. Polym. Sci. 104 (2007) 4053-4059.
[16] Y. Zhang, K.J. Balkus Jr, I.H. Musselman, J.P. Ferraris, Mixed-matrix membranes composed of Matrimid® and mesoporous ZSM-5 nanoparticles, J. Membr. Sci. 325 (2008) 28-39.
[17] S. Husain, W.J. Koros, Macrovoids in Hybrid Organic/Inorganic Hollow Fiber Membranes, Ind. Eng. Chem. Res. 48 (2009) 2372-2379.
[18] E.M. Flanigen, J.M. Bennett, R.W. Grose, J.P. Cohen, R.L. Patton, R.M. Kirchner, J.V. Smith, Silicalite, a new hydrophobic crystalline molecular-sieve, Nature 271 (1978) 512-516.
[19] A. Bos, I.G.M. Punt, M. Wessling, H. Strathmann, CO2-induced plasticization phenomena in glassy polymers, J. Membr. Sci. 155 (1999) 67-78.
[20] A. Pihlajamäki, P. Väisänen, M. Nyström, Characterization of clean and fouled polymeric ultrafiltration membranes by Fourier transform IR spectroscopy-attenuated total reflection, Colloids Surf. A 138 (1998) 323-333.
[21] P. Musto, M. Abbate, M. Lavorgna, G. Ragosta, G. Scarinzi, Microstructural features, diffusion and molecular relaxations in polyimide/silica hybrids, Polymer 47 (2006) 6172-6186.
[22] D.H. Olson, G.T. Kokotailo, S.L. Lawton, W.M. Meier, Crystal-structure and structure-related properties of ZSM-5, Journal of Physical Chemistry 85 (1981) 2238-2243.
[23] V. Wernert, O. Schaf, V. Faure, P. Brunet, L. Dou, Y. Berland, P. Boulet, B. Kuchta, R. Denoyel, Adsorption of the uremic toxin p-cresol onto hemodialysis membranes and microporous adsorbent zeolite silicalite, J. Biotechnol. 123 (2006) 164-173.
[24] I.F.J. Vankelecom, S. VandenBroeck, E. Merckx, H. Geerts, P. Grobet, J.B. Uytterhoeven, Silylation to improve incorporation of zeolites in polyimide films, J. Phys. Chem. 100 (1996) 3753-3758.
[25] P. Gorgojo, S. Uriel, C. Téllez, J. Coronas, Development of mixed matrix membranes based on zeolite Nu-6(2) for gas separation, Microporous Mesoporous Mater. 115 (2008) 85-92.
[26] M. Moaddeb, W.J. Koros, Gas transport properties of thin polymeric membranes in the presence of silicon dioxide particles, J. Membr. Sci. 125 (1997) 143-163.
[27] W.J.W. Bakker, L.J.P. vandenBroeke, F. Kapteijn, J.A. Moulijn, Temperature dependence of one-component permeation through a silicalite-1 membrane, AIChE J. 43 (1997) 2203-2214.

[28] S.S. Hosseini, M.M. Teoh, T.S. Chung, Hydrogen separation and purification in membranes of miscible polymer blends with interpenetration networks, Polymer 49 (2008) 1594-1603.
[29] L. Shao, L. Liu, S.X. Cheng, Y.D. Huang, J. Ma, Comparison of diamino cross-linking in different polyimide solutions and membranes by precipitation observation and gas transport, J. Membr. Sci. 312 (2008) 174-185.
[30] J.S. McHattie, W.J. Koros, D.R. Paul, Gas-transport properties of polysulfones. 1. Role of symmetry of methyl-group placement on bisphenol rings, Polymer 32 (1991) 840-850.
[31] J. Ahn, W.-J. Chung, I. Pinnau, M.D. Guiver, Polysulfone/silica nanoparticle mixed-matrix membranes for gas separation, J. Membr. Sci. 314 (2008) 123-133.
[32] S. Kim, E. Marand, J. Ida, V.V. Guliants, Polysulfone and mesoporous molecular sieve MCM-48 mixed matrix membranes for gas separation, Chem. Mater. 18 (2006) 1149-1155.
[33] Y. Zhang, I.H. Musselman, J.P. Ferraris, K.J. Balkus Jr, Gas permeability properties of Matrimid® membranes containing the metal-organic framework Cu-BPY-HFS, J. Membr. Sci. 313 (2008) 170-181.
[34] M.P. Bernal, M. Bardaji, J. Coronas, J. Santamaria, Facilitated transport of O2 through alumina-zeolite composite membranes containing a solution with a reducible metal complex, J. Membr. Sci. 203 (2002) 209-213.
[35] V. Sebastian, I. Kumakiri, R. Bredesen, M. Menendez, Zeolite membrane for CO2 removal: Operating at high pressure, J. Membr. Sci. 292 (2007) 92-97.
[36] C.L. Aitken, W.J. Koros, D.R. Paul, Effect of structural symmetry on gas-transport properties of polysulfones, Macromolecules 25 (1992) 3424-3434.
[37] J.A. Dunne, R. Mariwala, M. Rao, S. Sircar, R.J. Gorte, A.L. Myers, Calorimetric Heats of Adsorption and Adsorption Isotherms. 1. O2, N2, Ar, CO2, CH4, C2H6, and SF6 on Silicalite, Langmuir 12 (1996) 5888-5895.
[38] P.Y. Li, F.H. Tezel, Equilibrium and kinetic analysis of CO2-N-2 adsorption separation by concentration pulse chromatography, J. Colloid Interf. Sci. 313 (2007) 12-17.
[39] M.P. Bernal, J. Coronas, M. Menéndez, J. Santamaría, Separation of CO2/N2 Mixtures Using MFI-Type Zeolite Membranes, AIChE Journal 50 (2004) 127-135.
[40] I. Langmuir, The constitution and fundamental properties of solids and liquids Part I Solids, J. Am. Chem. Soc. 38 (1916) 2221-2295.

Figure captions

Figure 1. SEM images of: a) MSS and b) HZS, and TEM images of: c) HZS and d) inset of c) with a, b and c crystal dimensions.

Figure 2. Cross-section SEM or TEM images of: (a), (b) and (c) 8 wt % HZS-PSF MMMs; (d) 8 wt % HZS-PI MMM.

Figure 3. Cross-section SEM images of: (a) 8 wt % HZS-PSF MMM; (b) 16 wt % HZS-PSF MMM; (c) 8 wt % HZS-PI MMM; (d) 8 wt % silicalite-1-PSF MMM.

Figure 4. H_2/CH_4 selectivity as a function of H_2 permeability for 0, 4, 8, and 16 wt % HZS-PSF and HZS-PI MMMs. For comparison, 8 wt % S1C-PSF, S1C-PI and MSS-PSF[21] MMMs are also depicted.

Figure 5. CO_2/N_2 selectivity as a function of CO_2 permeability for 0, 4, 8, and 16 wt % HZS-PSF and HZS-PI MMMs. For comparison, 8 wt % S1C-PSF, S1C-PI and MSS-PSF[21] MMMs are also depicted.

Figure 6. O_2/N_2 selectivity as a function of O_2 permeability for 0, 4, 8, and 16 wt % HZS-PSF and HZS-PI MMMs. For comparison, 8 wt % S1C-PSF and S1C-PI MMMs are also depicted.

Figure 7. SEM image of 8 wt % HZS-PSF MMM. The thick and thin white arrows represents H_2, CO_2 and O_2 transport (that of the faster permeating molecule in each binary mixture) through the HZS and PSF media in the H_2/CH_4, CO_2/N_2 and O_2/N_2 mixtures, while the thinner black arrows represents CH_4 and N_2 in the same mixtures through the HZS and PSF media, respectively.

Figure 8. Experimental (symbols) and calculated (lines) adsorption isotherms for O_2, N_2, CH_4 and CO_2 on hollow silicalite-1 spheres (HZSs). In the inset: q_M (mmol/g) and K_A (kPa^{-1}) for each gas, according to the Langmuir model. Temperature= 35 ºC.

Figure 9. Experimental (symbols) and calculated (lines) CO_2 adsorption isotherms for S1C (about 1-2 μm silicalite-1 crystals), MSS (mesoporous silica spheres), HZS (hollow silicalite-1 spheres). In the inset: q_M (mmol/g) and K_A (kPa^{-1}) for each material, according to the Langmuir model. Temperature= 35 ºC.

Table 1. HZS actual loading (AL) and glass transition temperature (T_g) as a function of nominal HZS mass fraction for HZS-PSF and HZS-PI MMMs. T_g values are given with their standard deviation of at least two different samples

	PSF-MMM		PI-MMM	
HZS wt %	**AL [wt %]**	**T_g [ºC]**	**AL [wt %]**	**T_g [ºC]**
0	-	188.5 (±0.8)	-	316.7 (±1.8)
4	4.5	192.6 (±1.0)	4.1	331.7 (±1.5)
8	8.2	195.1 (±1.4)	7.8	339.8 (±1.1)
16	16.3	196.7 (±1.2)	15.7	342.2 (±1.2)

Table 2. Comparison of the maximum selectivities obtained here with those corresponding to pure polymers and MMMs comprising MFI-type zeolite (ZSM-5). Polymers: PSF and PI.

H_2/CH_4 mixture		
Membrane	**H_2 permeability (Barrer)**	**H_2/CH_4 selectivity**
Pure PSF [30,31]	11.8	53.6
Pure PSF [this work]	11.8	58.9
8 wt % HZS-PSF [this work]	15.4	80.3
Pure PI [28,29]	17.5-27.2	83.3-129
Pure PI [this work]	30.4	132
8 wt % HZS-PI [this work]	38.4	180
10 wt % ZSM-5-PI [16]	23.1	82.6
CO_2/N_2 mixture		
Membrane	**CO_2 permeability (Barrer)**	**CO_2/N_2 selectivity**
Pure PSF [8,30,31]	4.5-6.3	22.4-26.2
Pure PSF [this work]	5.9	24.3
8 wt % HZS-PSF [this work]	7.2	41.7
Pure PI [16,28,29]	6.5-7.3	25.0-33.1
Pure PI [this work]	7.6	26.6
8 wt % HZS-PI [this work]	18.7	39.8
10 wt % ZSM-5-PI [16]	9.0	26.5
CO_2/N_2 mixture		
Membrane	**O_2 permeability (Barrer)**	**O_2/N_2 selectivity**
Pure PSF [8,3031]	0.98-1.4	5.4-5.8
Pure PSF [this work]	1.6	4.7
8 wt % HZS-PSF [this work]	2.3	6.9
Pure PI [16,28,29]	1.5-1.7	6.0-6.6
Pure PI [this work]	1.9	5.5
8 wt % HZS-PI [this work]	2.8	8.5
10 wt % ZSM-5-PI [16]	1.7	5.0

Table 3. Summary of the advantages of the HZS-MMMs prepared here.

Filler (HZS) properties	Advantages of HZS-MMMs (vs. pure polymers or other MMMs)
Regular microporosity (~ 5.5 Å)	Increase in H_2/CH_4, CO_2/N_2 and O_2/N_2 selectivities
External specific surface area (~ 100 m^2/g)	Good filler-polymer contact
Spherical shape	Good dispersion, low loading needed
Hollow nature	Increase in gas permeability, potential application in other fields

Comentado [F1]: Decir algo del tamaño de las particulas micrométricas?

Comentado [F2]: Poner algún ejemplo

Figure 1

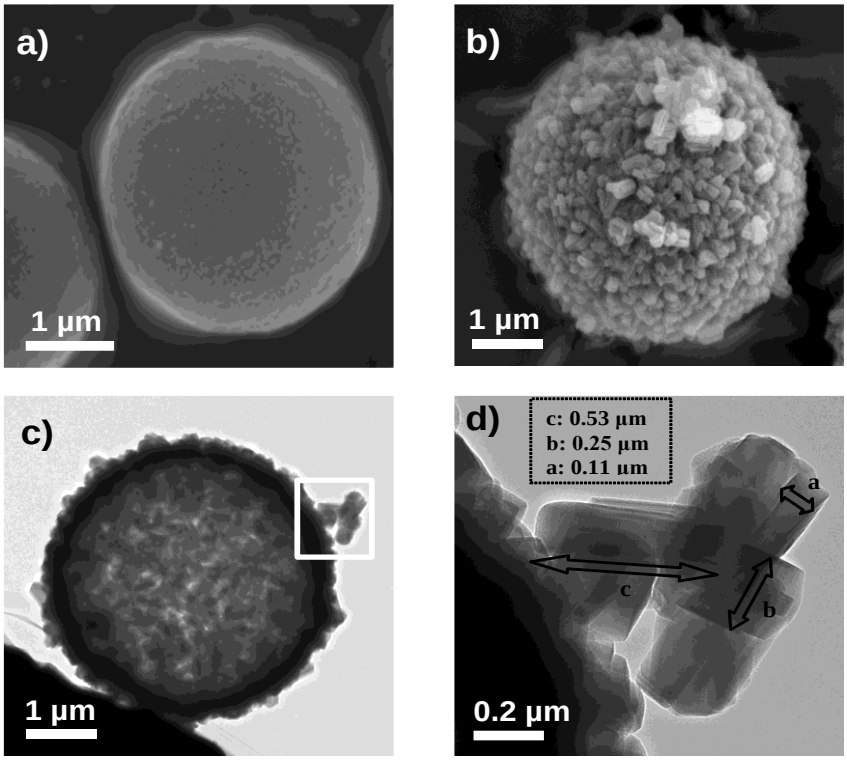

Figure 2

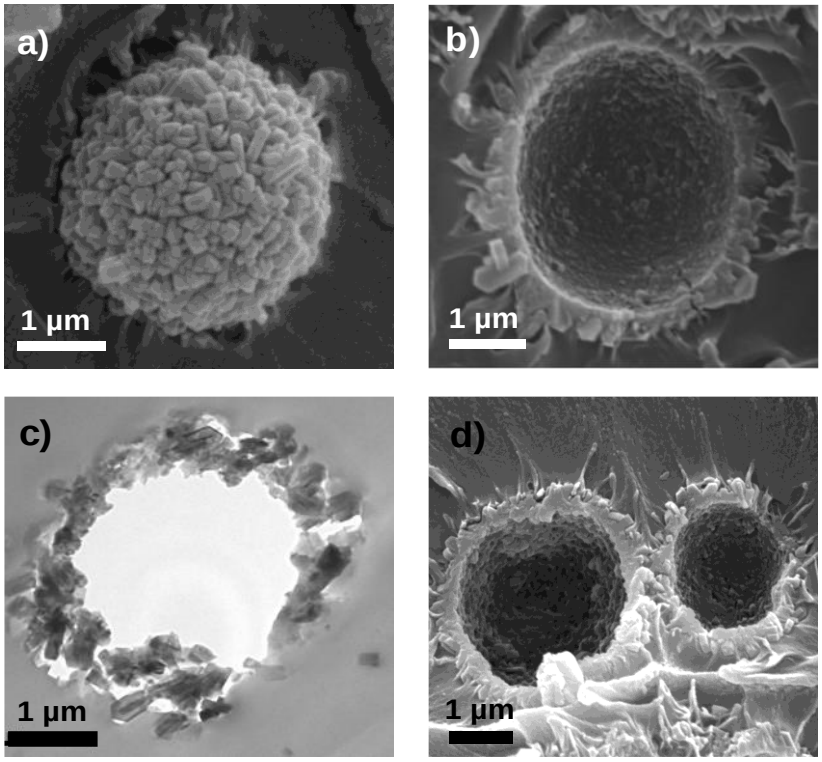

Figure 3

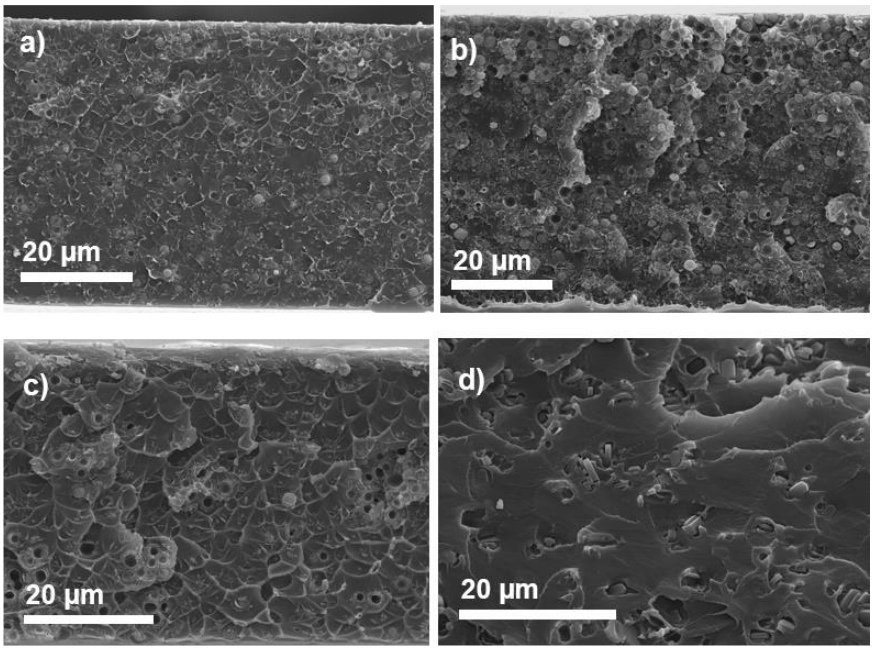

Figure 4

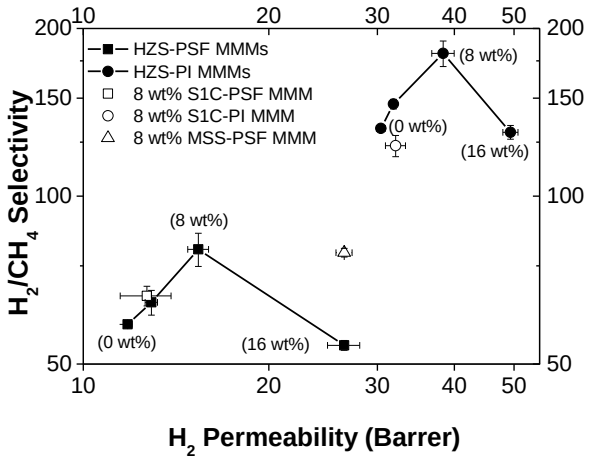
HZS-PSF MMMs
HZS-PI MMMs
8 wt% S1C-PSF MMM
8 wt% S1C-PI MMM
8 wt% MSS-PSF MMM
(8 wt%)
(0 wt%)
(16 wt%)
(8 wt%)
(0 wt%)
(16 wt%)
H2/CH4 Selectivity
H2 Permeability (Barrer)
10
20
30
40
50
100
150
200

Figure 5

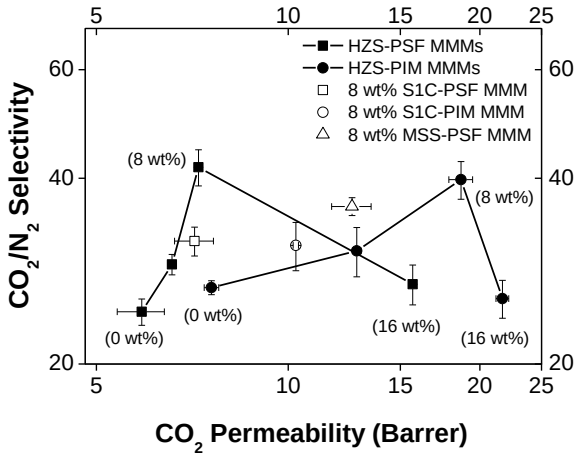
HZS-PSF MMMs
HZS-PIM MMMs
8 wt% S1C-PSF MMM
8 wt% S1C-PIM MMM
8 wt% MSS-PSF MMM
(8 wt%)
(8 wt%)
(0 wt%)
(0 wt%)
(16 wt%)
(16 wt%)
CO2/N2 Selectivity
CO2 Permeability (Barrer)
5
10
15
20
25
20
40
60

Figure 6

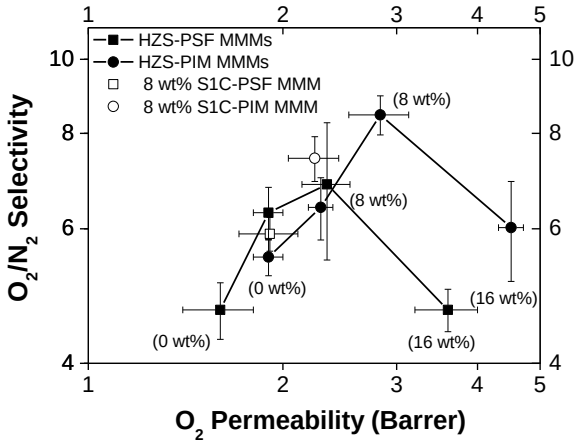
HZS-PSF MMMs
HZS-PIM MMMs
8 wt% S1C-PSF MMM
8 wt% S1C-PIM MMM
(8 wt%)
(8 wt%)
(0 wt%)
(0 wt%)
(16 wt%)
(16 wt%)
O2/N2 Selectivity
O2 Permeability (Barrer)
1
2
3
4
5
4
6
8
10

Figure 7

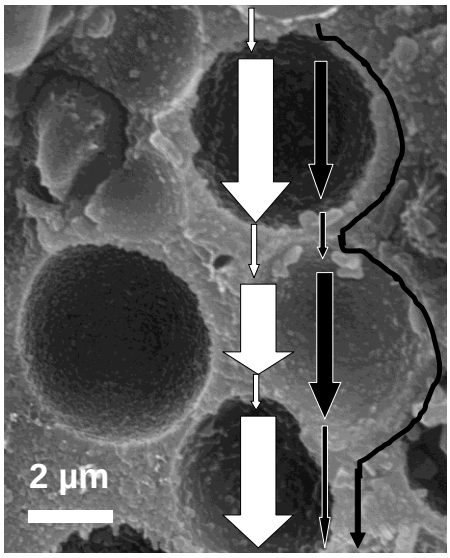

Figure 8

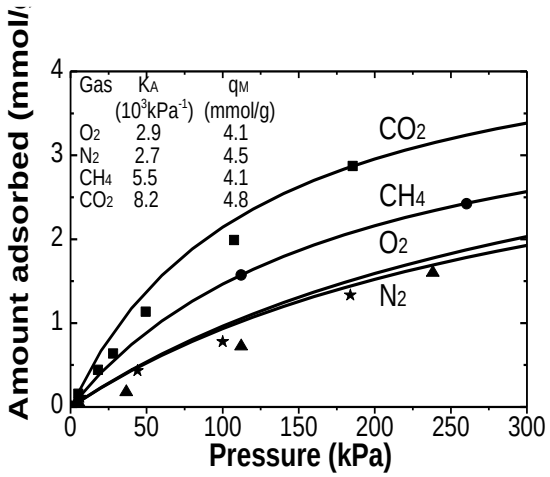
Amount adsorbed (mmol/
Pressure (kPa)
Gas K_A (10^3kPa^-1) q_M (mmol/g)
O2 2.9 4.1
N2 2.7 4.5
CH4 5.5 4.1
CO2 8.2 4.8
CO2
CH4
O2
N2
0
1
2
3
4
0
50
100
150
200
250
300

Figure 9

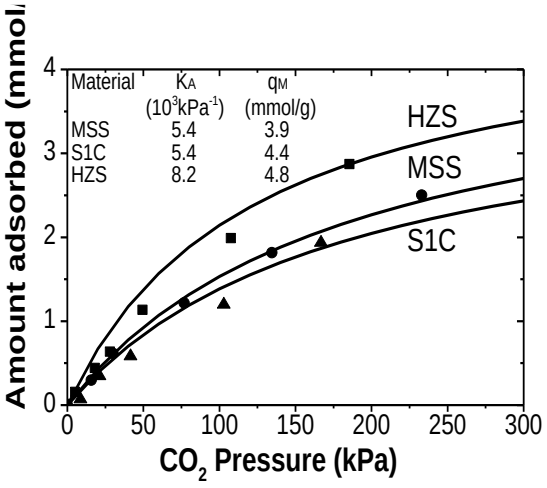
Amount adsorbed (mmol
Material
K_A (10^3kPa^{-1})
q_M (mmol/g)
MSS 5.4 3.9
S1C 5.4 4.4
HZS 8.2 4.8
HZS
MSS
S1C
0
1
2
3
4
0
50
100
150
200
250
300
CO_2 Pressure (kPa)